# 3–Dimensional Lattice Studies of the Electroweak Phase Transition at $M_{Higgs} \approx 70$ GeV

M. Gürtler[1]*, E.-M. Ilgenfritz[2]†, J. Kripfganz[3]‡
H. Perlt[1]§ and A. Schiller[1]¶

[1] *Institut für Theoretische Physik, Universität Leipzig, Germany*
[2] *Institut für Physik, Humboldt-Universität zu Berlin, Germany*
[3] *Institut für Theoretische Physik, Universität Heidelberg, Germany*

May 31, 1996

## Abstract

We study the electroweak phase transition by lattice simulations of an effective 3–dimensional theory, for a Higgs mass of about 70 GeV. Exploiting, among others, a variant of the equal weight criterion of phase equilibrium, we obtain transition temperature, latent heat and surface tension, and compare with $M_H \approx 35$ GeV. In the broken phase masses and Higgs condensates are compared to perturbation theory. For the symmetric phase, bound state masses and the static force are determined.
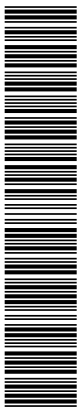
*guertler@tph204.physik.uni-leipzig.de
†ilgenfri@pha2.physik.hu-berlin.de
‡j.kripfganz@thphys.uni-heidelberg.de
§perlt@tph204.physik.uni-leipzig.de
¶schiller@tph200.physik.uni-leipzig.de

# 1 Introduction

Recent lattice studies of the electroweak phase transition [1]-[8] had been triggered by the interest in understanding the baryon number asymmetry of the universe. Significant cosmological consequences would require a sufficiently strong first order transition [9, 10]. The transition has to be strong enough, both in order to accomplish a sufficient rate of baryon generation during the transition and to prevent the wash–out of baryon number after it is completed. The present quantitative understanding of possible mechanisms as well as experimental lower bounds for the Higgs mass make this unlikely within the minimal standard model. Extensions, in particular supersymmetric ones may still be viable, however [11]-[13].

A second reason for lattice investigations was the wish to control the behaviour of perturbative calculations of the effective action. This quantity is the appropriate tool of (non–lattice) thermal quantum field theory for dealing with symmetry breaking. Infrared problems prevent a perturbative evaluation of the free energy in the symmetric phase to higher loop order. However, the true, non–perturbative nature of the symmetric phase will be characterized by massive $W-$ and Higgs bound states instead of massless $W$ gauge bosons. A self–consistent approach to provide masses across the transition, $e.g.$ by gap equations [14], can improve the ability to calculate perturbatively the symmetric phase. Gauge field condensates are another property of the symmetric phase, expected to lower its free energy density.

An independent method is needed to characterize the electroweak phase transition even within a pure $SU(2)$ gauge–Higgs version of the theory. This model has become a test–field to control the validity of perturbative predictions over a broad range of Higgs masses. At present, one is interested to see whether the first order transition ends somewhere around a Higgs mass $M_H \approx 100$ GeV [15, 16]. Lattice simulations are not only able to describe both phases starting from first principles but, moreover, make it possible to put both phases into coexistence near the phase equilibrium. Thus one is able to measure directly quantities like latent heat, surface tension, condensates etc. quantifying the strength of the transition.

One approach to lattice calculations of the electroweak transition is based on an effective 3–dimensional Higgs model. It is attractive phenomenologically because it circumvents the problem of putting chiral fermions on the lattice. Due to dimensional reduction, fermions as well as non–static bosonic modes contribute to the effective action. In contrast to QCD, dimensional reduction should work for the electroweak theory around and above the transition temperature because $g^2$ is small. For the electroweak phase transition this approach has been pioneered by Farakos et al. (see $e.g.$ [17, 18]). This program aims

at exploring the accuracy of dimensional reduction at various Higgs masses by comparing various parameters of the transition with those of 4–dimensional lattice and perturbative approaches. Perturbation theory is necessary to relate the 4–dimensional continuum theory to the parameters of the dimensionally reduced theory and, finally, to the bare coupling parameters of the lattice action. Dimensionally reduced versions retain the remnant of the temporal gauge field $A_0$ (as an adjoint Higgs field) or not (as in this work).

In its simplest version the dimensionally reduced effective theory is again a $SU(2)$–Higgs theory with just one doublet. This model represents whole classes of $4d$ theories but might not be sufficient to describe all $4d$ variants generically. So far, only this simple effective theory has been studied by lattice techniques, for several Higgs self–couplings $\lambda_3$ in units of the $3d$ gauge couplings squared $g_3^2$ [5, 7, 6, 8]. Here we extend our analysis [6] to a higher coupling value

$$\frac{\lambda_3}{g_3^2} = \frac{1}{8}\left(\frac{M_H^*}{80\ \mathrm{GeV}}\right)^2 \tag{1}$$

namely $\lambda_3/g_3^2 \approx 0.095703$, referred to as $M_H^* = 70$ GeV, and compare with previous results at this smaller coupling $\lambda_3/g_3^2 \approx 0.023926$ ($M_H^* = 35$ GeV). As expected the first order nature has become weaker but is still evident.

## 2 Relation of the dimensionally reduced model to the $SU(2)$ Higgs theory in four dimensions

The procedure of dimensional reduction in gauge theories consists of two steps. In a first step, nonstatic modes of the gauge field are integrated while the temporal component $A_0$ is retained as adjoint Higgs field. The action is further simplified by integrating over $A_0$ in a second step. The mass of the latter field is given by the Debye mass $m_D$. The reduced Higgs theory has the following action resembling the form of the 4–dimensional theory

$$S = \int d^3x \left(\frac{1}{4}F_{\alpha\beta}^b F_{\alpha\beta}^b + (D_\alpha\phi)^+(D_\alpha\phi) + m_3^2\phi^+\phi + \lambda_3(\phi^+\phi)^2\right), \tag{2}$$

where $\alpha, \beta, b = 1, 2, 3$. The 3–dimensional mass parameter $m_3(\mu_3)$, renormalized at scale $\mu_3$ and the renormalization group invariant couplings $\lambda_3$ and $g_3$ can be expressed by dimensional mapping in terms of the running parameters of the 4–dimensional theory at the scale $\mu$ and temperature $T$ in the $\overline{MS}$ scheme. The renormalization scale $\mu$ is most conveniently chosen as $\mu = \mu_T = 7.05T$ which puts logarithmic contributions of bosonic origin to zero.

To make this paper self–contained we collect some formulae for later use. As the result of the second step of reduction mentioned above, the couplings $g_3$ and $\lambda_3$ and the 3–dimensional mass $m_3$ can be expressed in terms of the corresponding couplings and mass of the intermediate theory with $A_0$ included, $\overline{g}_3$, $\overline{\lambda}_3$ and $\overline{m}_3$ (and the Debye mass $m_D = \sqrt{5/6}gT$). The latter parameters in their turn can be written in terms of the temperature and the parameters of the 4–dimensional theory:

$$
\begin{aligned}
g_3^2 &= \overline{g}_3^2\big(1 - \frac{\overline{g}_3^2}{24\pi m_D}\big), \\
\overline{g}_3^2 &= g^2(\mu_T)\ T\ \big(1 + \frac{g^2}{16\pi^2}\frac{2}{3}\big), \\
\lambda_3 &= \overline{\lambda}_3 - \frac{3\overline{g}_3^4}{128\pi m_D}, \\
\overline{\lambda}_3 &= \lambda(\mu_T)\ T\ \big(1 + \frac{g^2}{16\pi^2}\frac{3M_W^2}{M_H^2}\big), \\
m_3^2(\mu_3) &= \overline{m}_3^2(\mu_3) - \frac{3}{16\pi}\overline{g}_3^2 m_D + \frac{\overline{g}_3^4}{16\pi^2}\big(\frac{15}{8}\log\frac{\mu_3}{2m_D} + \frac{9}{16}\big), \\
\overline{m}_3^2(\mu_3) &= -\nu^2(\mu_T) + T\big(\frac{1}{2}\overline{\lambda}_3 + \frac{3}{16}\overline{g}_3^2\big) + \frac{T^2}{16\pi^2}\big(\frac{137}{96}g^4 + \frac{3}{4}\lambda g^2\big) \\
&\quad + \frac{1}{16\pi^2}\big(\frac{81}{16}\overline{g}_3^4 + 9\overline{\lambda}_3\overline{g}_3^2 - 12\overline{\lambda}_3^2\big)\big(\log\frac{3T}{\mu_3} - 0.348725\big).
\end{aligned}
\tag{3}
$$

The 4–dimensional renormalized quantities $g^2(\mu)$ , $\nu^2(\mu)$ and $\lambda(\mu)$ have the generic form with one–loop corrections formally indicated

$$
\begin{aligned}
g^2(\mu_T) &= g_0^2(1 + \delta g^2) \\
\lambda(\mu_T) &= \frac{g_0^2}{8}\frac{M_H^2}{M_W^2}(1 + \delta\lambda) \\
\nu^2(\mu_T) &= \frac{M_H^2}{2}(1 + \delta\nu^2)
\end{aligned}
\tag{4}
$$

with $g_0^2 = 4\sqrt{2}G_F M_W^2$. $G_F = 1.16639 \times 10^{-5} \mathrm{GeV}^{-2}$ is Fermi's constant. The corrections indicated in these formulae, which depend on $g^2$, $\mu_T$ and the Higgs and $W$ mass squared $M_H^2$ and $M_W^2$, can be found in Ref. [18]. For definiteness, we use as the 3–dimensional renormalization scale $\mu_3 = g_3^2$ and take $M_W = M_Z = 80.6$ GeV. For the 4–dimensional coupling in the loop corrections we choose $g^2 = g_0^2$.

At $M_H^* = 70$ GeV the corrections in (4) without fermions are numerically obtained as follows

$$
\begin{aligned}
\delta g^2 &\approx -0.01343 - 0.01945 \log(\mu_T^2/M_W^2), \\
\delta \lambda &\approx -0.01625 + 0.008491 \log(\mu_T^2/M_W^2), \\
\delta \nu^2 &\approx -0.01892 - 0.004721 \log(\mu_T^2/M_W^2).
\end{aligned}
\tag{5}
$$

Similarly, we find for $M_H^* = 35$ GeV

$$
\begin{aligned}
\delta g^2 &\approx -0.01281 - 0.01945 \log(\mu_T^2/M_W^2), \\
\delta \lambda &\approx -0.05396 + 0.06131 \log(\mu_T^2/M_W^2), \\
\delta \nu^2 &\approx -0.07286 - 0.005766 \log(\mu_T^2/M_W^2).
\end{aligned}
\tag{6}
$$

# 3 The 3–dimensional lattice model

## 3.1 Lattice action

On the lattice, we study the $SU(2)$–Higgs system with one complex Higgs doublet of variable modulus. The gauge field is represented by unitary $2 \times 2$ link matrices $U_{x,\alpha}$ and the Higgs fields are written as $\Phi_x = \rho_x V_x$. $\rho_x^2 = \frac{1}{2} Tr(\Phi_x^+ \Phi_x)$ is the Higgs modulus squared, $V_x$ an element of the group $SU(2)$, $U_p$ denotes the $SU(2)$ plaquette matrix. The lattice action is

$$
\begin{aligned}
S &= \beta_G \sum_p \left(1 - \frac{1}{2} Tr U_p\right) - \beta_H \sum_l \frac{1}{2} Tr(\Phi_x^+ U_{x,\alpha} \Phi_{x+\alpha}) \\
&\quad + \sum_x \left(\rho_x^2 + \beta_R (\rho_x^2 - 1)^2\right)
\end{aligned}
\tag{7}
$$

(summed over plaquettes $p$, links $l$ and sites $x$), with

$$
\beta_G = \frac{4}{a g_3^2}.
\tag{8}
$$

The lattice Higgs self–coupling is

$$
\beta_R = \frac{\lambda_3}{g_3^2} \frac{\beta_H^2}{\beta_G}
\tag{9}
$$

5

and the hopping parameter can be expressed in the form

$$\beta_H = \frac{2(1 - 2\beta_R)}{6 + a^2 m_3^2}.$$
(10)

The relation between the 3−dimensional bare mass squared $m_3^2$, expressed via the lattice couplings (see (10)) and the renormalized continuum mass squared has been worked out by Laine [19] to two loops

$$
\begin{aligned}
m_3^2(\mu_3) &= m_3^2 + m_1^2 + m_2^2 \\
m_1^2 &= \frac{\Sigma}{4\pi a}(\frac{3}{2}g_3^2 + 6\lambda_3) , \quad \Sigma = 3.175911 \\
m_2^2 &= \frac{1}{16\pi^2}((\frac{51}{16}g_3^4 + 9\lambda_3 g_3^2 - 12\lambda_3^2)(\log\frac{6}{a\mu_3} + 0.09) \\
&\quad + 5.0g_3^4 + 5.2\lambda_3 g_3^2).
\end{aligned}
$$
(11)

This completes the relation of the lattice parameters of the $3d$ model to the $4d$ continuum parameters.

The lattice model defined by (7) is numerically studied at given couplings $\beta_G$, $\beta_H$ and $\lambda_3/g_3^2$. We have used the same simulation algorithms as in our previous investigations. We have combined a 3−dimensional Gaussian heat bath update for the gauge fields with a 4−dimensional Gaussian heat bath method for the Higgs field. In the last one, the Gaussian step was improved for later acceptance by taking the non−linearity into account. To reduce the autocorrelations near to the phase transition, a heat bath step as described was followed by several reflections (eight in practice) for the Higgs (and partly one reflection for the gauge field).

In the search for the phase transition, bulk variables like the space−averaged square of the Higgs modulus and the space−average link

$$
\begin{aligned}
\rho^2 &= \frac{1}{L_x L_y L_z}\sum_x \rho_x^2, \\
E_{link} &= \frac{1}{3L_x L_y L_z}\sum_{x,\alpha}\frac{1}{2}Tr(\Phi_x^+ U_{x,\alpha}\Phi_{x+\alpha}),
\end{aligned}
$$
(12)

are heavily used (the average quartic Higgs modulus $\rho^4$ is defined analogously). Others like the average plaquette

$$P = \frac{1}{3L_x L_y L_z}\sum_p \frac{1}{2}TrU_p$$
(13)

6

are less useful for this purpose, although they also show a two–state signal on large enough lattices. In principle, the histograms and discontinuities of all bulk variables have to be known in order to estimate the strength of the phase transition, but $\rho^2$ proves to be the most important one. It has turned out that, due to the confinement property of the symmetric phase, histograms of medium size rectangular Wilson loops show a two–state signal as well.

While the bulk quantities discussed are measured after each Monte Carlo iteration, other quantities like Wilson loops and correlation functions are measured after every 10th iteration.

To reduce the noise in the evaluation of Wilson loops the original links are replaced by their mean field values [20]. They are calculated from the links interacting with the original links through the staples. In the case of $SU(2)$ this value is calculated analytically. This procedure is not applied to the links in the corners of the Wilson loops.

The Higgs and vector boson masses are measured from correlation functions of extended operators of length n ($\tau^b$ are the Pauli matrices)

$$0^+ \quad : \quad S_{x,\alpha}(n) = \frac{1}{2}Tr(\Phi_x^+ U_{x,\alpha}U_{x+\alpha,\alpha}\ldots U_{x+(n-1)\alpha,\alpha}\Phi_{x+n\alpha})$$

$$1^- \quad : \quad V_{x,\alpha}^b(n) = \frac{1}{2}Tr(\tau^b\Phi_x^+ U_{x,\alpha}U_{x+\alpha,\alpha}\ldots U_{x+(n-1)\alpha,\alpha}\Phi_{x+n\alpha}) \quad (14)$$

For the mass fits we have used the maximum $n(=4)$ for the vector boson which gave the best signal in the symmetric phase. In the Higgs channel we did not observe such a strong $n$ dependence. In the analysis we used both $n = 0$ and $n = 4$.

## 3.2 Implementation on QUADRICS parallel computers

The simulations which are reported in this paper have been performed on QUADRICS parallel computers at the University of Bielefeld, at the QUADRICS Q4o and the CRAY-YMP of HLRZ in Jülich. Additionally, codes have been partly tested on the Q1 at DESY–IfH Zeuthen. The computing facilities at Bielefeld were provided by the Deutsche Forschungsgemeinschaft (DFG) to the groups being part of the DFG task force program "Dynamical Fermions". The code written in TAO had to be portable to various topologies of the QUADRICS family (Q4o, QH2) of parallel machines. The Q4o is a 32 node machine with a $2 \times 4 \times 4$ topology, the QH2 has 256 nodes in $4 \times 8 \times 8$ topology.

For the calculation of large Wilson loops we have defined long strings of links and their mean field values (as auxiliary field attached to the point of

beginning). The factors must be communicated from remote processor nodes. Forming loops in a later step, these auxiliary building blocks must be multiplied non–locally where nodes far away have to be addressed simultaneously. Due to memory constraints (size of the auxiliary field) we were able to measure Wilson loops on the Q4o for lattice sizes up to $40^3$. Similar communications have to be considered for correlation functions on non–neighbouring nodes.

The accumulation of histograms of bulk variables as well as Wilson loops must be done on the host computer (after taking the appropriate global sums which are then available on all nodes simultaneously) since integer arithmetics is not possible on the QUADRICS processors.

## 3.3  Multihistogram technique and phase separation

As usual, the search for the phase transition point requires extensive application of the multihistogram technique [21, 1] to the bulk variables listed above. We have processed data obtained in up to 7 runs with different $\beta_H$ values (for a given volume) within and near to the metastable region. Each run consisted out of 30000 to 145000 measurements, depending on the measured integrated autocorrelation time $\tau_{int}$. The respective maximum of the autocorrelation time increases roughly linearly with the volume. These numbers, observed in the run nearest to the respective pseudocritical $\beta_{Hc}$, range from 200 (for $30^3$) to 1500 (for $64^3$). These are autocorrelation times *with* tunneling and mainly indicate the longer lifetime of each one of the two metastable phases, *i.e.* the suppression of tunneling in the larger lattices.

We look for the phase transition point in terms of the critical hopping parameter, $\beta_{Hc}$, for various (in fact two, in the present work) values of the lattice gauge coupling $\beta_G$, while the continuum couplings are kept fixed. In other words, we have studied the phase transition driven by $m_3$. Then the lattice Higgs self–coupling $\beta_R$ varies with $\beta_H$ (see (9)). Therefore, the reweighting uses not only $E_{link}$, but $\rho^2$ and $\rho^4$ at the same time. In general, a 3–dimensional binning has to be performed in the two relevant parts of the action (corresponding to $\beta_H$ and $\beta_R$) and some other observable of interest. This enables to create histograms for any bulk variable and for any value of $\beta_H$ near to the transition point, based on an estimated density of states which subsums all measurements in the metastable region with appropriate weights.

We have determined the finite volume pseudocritical $\beta_{Hc}(L)$ by the minima of the Binder cumulants

$$B_{E_{link}}(L, \beta_H) = 1 - \frac{\langle E_{link}^4 \rangle}{3\langle E_{link}^2 \rangle^2} \tag{15}$$

8

and $B_{\rho^2}(L, \beta_H)$, by the maxima of the susceptibilities

$$C_{E_{link}}(L, \beta_H) = \langle E_{link}{}^2 \rangle - \langle E_{link} \rangle^2 \tag{16}$$

and $C_{\rho^2}(L, \beta_H)$, and using the equal weight method. Our aim is to apply this method for phase transitions of relatively weak first order. For these transitions a frequent tunneling between the pure phases is observed in the metastability region for all lattice sizes studied. This has made necessary the refinements described below.

Concerning histogram methods at first order transitions, there is an ambiguity in the literature how to define the critical coupling (in fact: pseudocritical for finite volume). Throughout the metastable region, a two–state signal is visible in the histograms, *e.g.* of $\rho^2$ and $E_{link}$, but there are *two* prescriptions for $\beta_{Hc}$: equal height of the maxima vs. equal weight of the two competing phases. While theoretical arguments [22] favour the equal weight criterion, this requires in practice a procedure to separate the (measured or reweighted) histogram into contributions from configurations to be attributed to the respective pure phases. In addition, there are inhomogeneous (mixed) configurations contributing to the histograms. There is no generally accepted procedure that unambiguously defines the weights of these three contributions.

Our main assumption is that the pure phases can be described by Gaussian distributions for any volume averaged quantity. Order parameters like $\rho^2$ or $E_{link}$ can be considered in this context. We have utilized the equal weight method as described below for the case of $\rho^2$. The normalized histogram has been presented as a weighted sum of three histograms referring to the two pure phases and to all inhomogeneous mixed states

$$p(\rho^2, \beta_H) = w_b p_b(\rho^2, \beta_H) + w_s p_s(\rho^2, \beta_H) + w_{mix} p_{mix}(\rho^2, \beta_H) \tag{17}$$

with

$$w_b + w_s + w_{mix} = 1. \tag{18}$$

$w_{b,s}$ denotes the weight of the broken/symmetric phase, $w_{mix}$ is the corresponding weight of the mixed state, all weights are $\beta_H$ dependent. The pseudocritical $\beta_{Hc}(L)$ is then found for $w_b = w_s < 0.5$.

The positions, widths and weights of the pure phase histograms at a given $\beta_H$ have been obtained by fitting the outer flanks of the two–peak histogram to Gaussian shape. At the same time, this fixes the weight $w_{mix}$ and the $\rho^2$ distribution to be attributed to configurations with domains of both phases in

equilibrium. We should mention potential additional problems to this fit procedure when histograms of both phases are strongly overlapping. In asymmetric transitions (generic for the Higgs case), with susceptibilities (widths) very different in both phases, this happens for smaller lattice sizes. For sufficiently large volumes one can avoid this problem.

We have used an iterative procedure to find the critical $\beta_{Hc}$ according to the requirement $w_b = w_s$. It consists of merging all data into a single histogram at a tentative $\beta_H$. This step is followed by a fitting procedure as described above which tells the weights of the pure phases at this $\beta_H$. If they are not equal, $\beta_H$ is corrected accordingly.

Phase separation of measurements is necessary not only for this application of the multihistogram method. Another particular example is the measurement of pure phase correlation lengths near to the phase transition. For this purpose and for the splitting of badly separating histograms in some particular variables it is better to use the Monte Carlo time sequence of configurations for runs in the metastability range. The aim is to remove successful tunneling escapes and unsuccessful tunneling attempts towards the "wrong" phase from what should then be considered as the Monte Carlo trajectory restricted to the "right" phase. The procedure rescans the records of the volume averaged $\rho^2$ which has a well separated two–peak signal for all considered volumes. Referring to this variable a lower cut for the upper (broken) phase and an upper cut for the lower (symmetric) phase can be chosen. These cuts are determined in such a way that the remaining histograms (for the "pure" phases) are almost symmetric around their maxima. If the Monte Carlo history of $\rho^2$ enters the range of a certain phase and stays there for more than 100 iterations, all measured quantities (recorded for the whole trajectory, including correlators etc.) are considered to contribute to the statistics of the given phase until the trajectory leaves this phase again.

The minimal time the trajectory is required to stay within one phase has to be much larger than the autocorrelation time *without* tunneling but smaller than the autocorrelation time *with* tunneling. The choice of 100 iterations is consistent with this requirement.

## 4   Localization of the phase transition

In Tables 1 and 2 the statistics is reported for each set of couplings and volumes, that has been used in the various procedures for the localization of the phase transition.

| $\beta_H$ | $30^3$ | $48^3$ | $64^3$ |
|---|---|---|---|
| 0.343440 | | 75000 | |
| 0.343480 | 30000 | | |
| 0.343520 | | 85000 | |
| 0.343540 | 50000 | 80000 | |
| 0.343544 | | 120000 | |
| 0.343546 | | | 90000 |
| 0.343548 | | 145000 | 120000 |
| 0.343550 | | | 100000 |
| 0.343560 | | 40000 | |
| 0.343580 | | 110000 | |
| 0.343600 | 40000 | | |

Table 1: Data samples used for the localization of the transition for $M_H^* = 70$ GeV and $\beta_G = 12$

| $\beta_H$ | $32^3$ | $40^3$ | $48^3$ |
|---|---|---|---|
| 0.340700 | | | 45000 |
| 0.340780 | 40000 | 40000 | 45000 |
| 0.340800 | 40000 | 100000 | 90000 |
| 0.343820 | 40000 | 40000 | 45000 |

Table 2: Data samples used for the localization of the transition for $M_H^* = 70$ GeV and $\beta_G = 16$

## 4.1 The infinite volume limit for $\beta_{Hc}$

In order to determine the set of pseudocritical values of the couplings $\beta_H$ (and the corresponding $\beta_R$) we have used the volume averages $\rho^2$ and $E_{link}$ searching for the minima of the Binder cumulants (15) $B_{\rho^2}(L, \beta_H)$ and $B_{E_{link}}(L, \beta_H)$, and for the maxima of the susceptibilities (16) $C_{\rho^2}(L, \beta_H)$ and $C_{E_{link}}(L, \beta_H)$. In addition to these methods we have used the equal weight method in the variant described above.

To demonstrate the two–peak structure we show in Fig. 1 the measured histogram of $\rho^2$ on lattices $48^3$ and $64^3$, all at $\beta_G = 12$, for $\beta_H$ values nearest to the respective pseudocritical $\beta_{Hc}(L)$. The positions of the maxima change already only slightly with the volume.

In Figs. 2 and 3 results of the multihistogram interpolation of our data for $\beta_G = 12$ for the Binder cumulant of $E_{link}$ and for the susceptibility of $\rho^2$ are presented. Finiteness and shrinking of the Binder cumulant with increasing volume present evidence for the first order nature of the transition at Higgs mass $M_H^* = 70$ GeV. The maximum of the interpolated susceptibility (with the
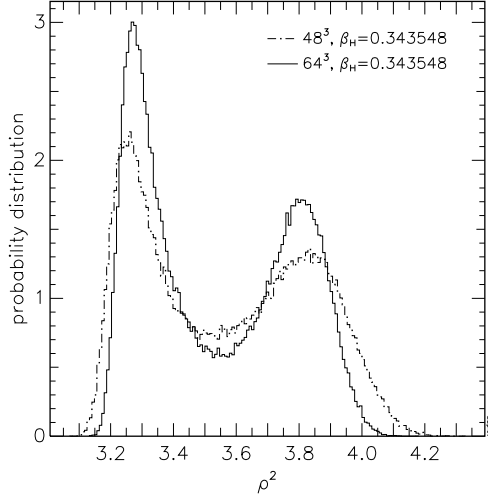
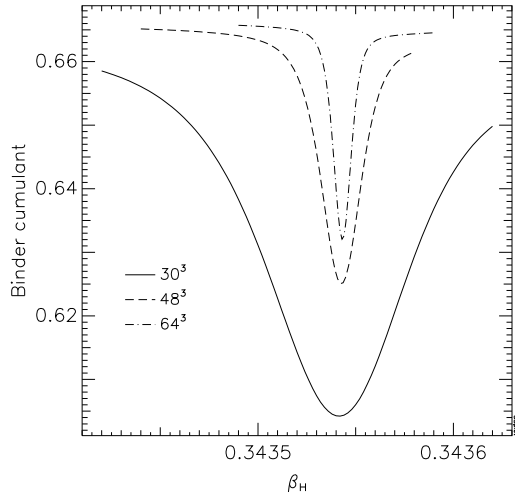Figure 1: *Measured histograms of $\rho^2$ for $\beta_G = 12$*



Figure 2: *Multihistogram interpolation of $B_{E_{link}}$, $\beta_G = 12$*

background susceptibility subtracted) increases almost linearly with the volume.

A histogram reweighted to pseudocritical $\beta_{Hc}(L) = 0.3435441$ (as determined according to the equal weight criterion) for a lattice size $64^3$ is presented in Fig. 4 together with the Gaussians describing the pure phases just at that $\beta_{Hc}$. The distribution attributed to mixed configurations with domains of both
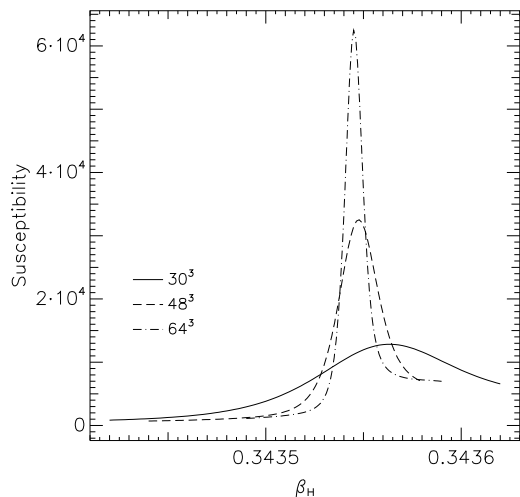
Figure 3: *Multihistogram interpolation of* $C_{\rho^2}$ *,* $\beta_G = 12$
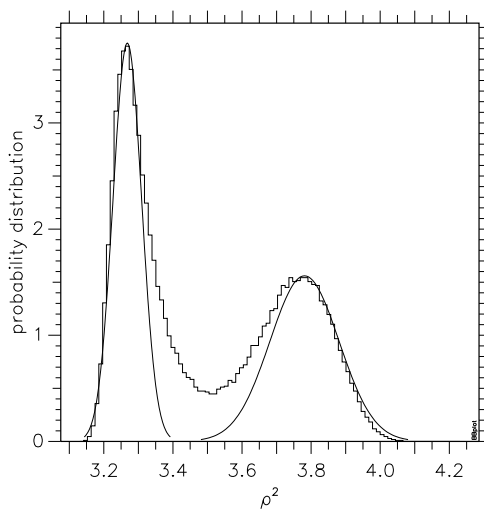


Figure 4: *Equal weight histogram of* $\rho^2$ *at pseudocritical* $\beta_H$*,* $\beta_G = 12$ *on a* $64^3$ *lattice with contributions of the pure phases*

phases in equilibrium is well identified between the two peaks.

The various pseudocritical $\beta_{Hc}(L)$ values for the three methods applied to $E_{link}$ and $\rho^2$ are collected in Figs. 5 and 6. They are plotted there versus $1/L^3$ for $\beta_G = 12$ and 16. The errors of the individual pseudocritical $\beta_H$ values
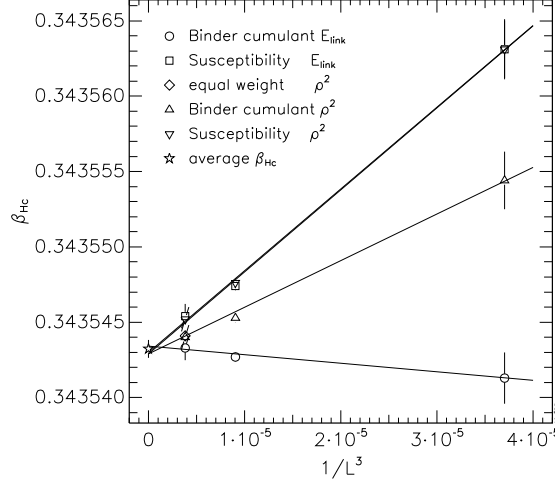
13

Figure 5: *Infinite volume extrapolation of $\beta_{Hc}$ for $\beta_G = 12$*
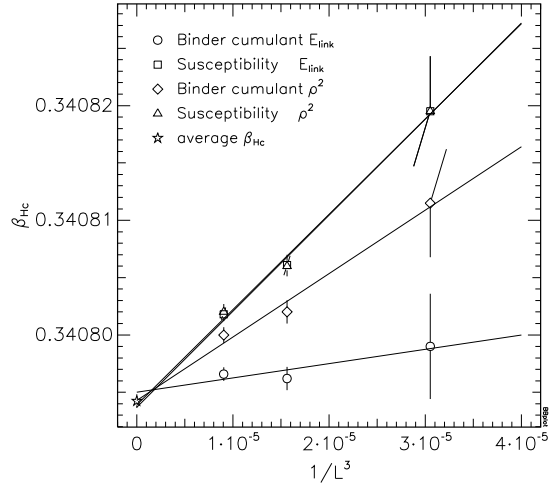


Figure 6: *Infinite volume extrapolation of $\beta_{Hc}$ for $\beta_G = 16$*

were obtained by a variant of the Jackknife procedure. From each of the Monte Carlo histories near to the critical point ($n$ simulated $\beta_H$ values, $n = 3$ in most cases) one half has been left out of the analysis. This amounts to $2^n$ Jackknife estimators for $\beta_{Hc}$. The equal weight method could be reasonably applied only for the larger volumes because of the overlap problem mentioned above. Corresponding to each method, a $1/L^3$ fit has been used to yield a

respective $\beta_{Hc}^{\infty}$. The extrapolations nicely coincide as expected.

In table 3 the extrapolations for each method are collected together with the average $\beta_{Hc}^{\infty}$ for $\beta_G = 12$ and 16. With the use of formulae (10,11,3,5) the $\beta_{Hc}^{\infty}$ is translated into a physical temperature and an "exact" Higgs mass $M_H$. For definiteness, these numbers are given for the case of the $SU(2)$ Higgs theory *without* fermions. Comparing these temperatures there seems to be not much space left for $O(a)$ corrections. The "exact" Higgs mass is practically the same.

| | $B$ | $C$ | $w_b = w_s$ |
|---|---|---|---|
| $\beta_G = 12$ | | | |
| $E_{link}$ | 0.3435434 | 0.3435430 | |
| $\rho^2$ | 0.3435429 | 0.3435429 | 0.3435441 |
| | | | |
| $\overline{\beta_{Hc}}$ | | 0.3435433(6) | |
| $T_c/\text{GeV}$ | | 154.34(1) | |
| $M_H/\text{GeV}$ | | 66.52 | |
| $\beta_G = 16$ | | | |
| $E_{link}$ | 0.3407950 | 0.3407937 | |
| $\rho^2$ | 0.3407943 | 0.3407939 | |
| | | | |
| $\overline{\beta_{Hc}}$ | | 0.3407942(6) | |
| $T_c/\text{GeV}$ | | 154.68(2) | |
| $M_H/\text{GeV}$ | | 66.52 | |

Table 3: Infinite volume limit for $\beta_{Hc}$ at $M_H^* = 70$ $GeV$

For comparison, at the smaller coupling ($M_H^* = 35$ GeV) the transition temperature is $T_c = 85.7(1)$ GeV with the Higgs mass $M_H = 33.0$ GeV. This has been obtained for gauge couplings in the range from $\beta_G = 12$ to 20 on lattices of size $40^3$ and $20^3$.

# 5 The strength of the phase transition

## 5.1 Condensate discontinuities at the phase transition

The jumps in $\langle \rho^2 \rangle$ and $\langle \rho^4 \rangle$ are connected to the renormalization group invariant discontinuities of the quadratic and quartic Higgs condensates. The two–state signal for $\langle \rho^2 \rangle$ and $\langle \rho^4 \rangle$ is still clearly visible for all lattice sizes considered at the higher Higgs mass of $M_H^* = 70$ GeV, where the transition turns out much

15

weaker than at $M_H^* = 35$ GeV. The continuum condensate jumps can be put into relation to the lattice quantities by the following formulae

$$\Delta\langle\phi^+\phi\rangle/g_3^2 = \frac{1}{8}\beta_G\beta_{Hc}\Delta\langle\rho^2\rangle \tag{19}$$

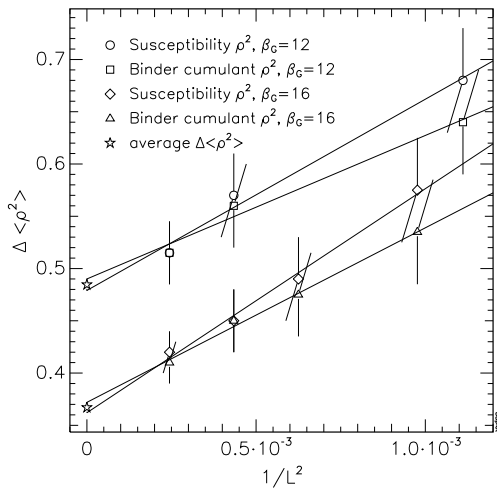$$\Delta\langle(\phi^+\phi)^2\rangle/g_3^4 = (\frac{1}{8}\beta_G\beta_{Hc})^2\Delta\langle\rho^4\rangle. \tag{20}$$



Figure 7: *Infinite volume extrapolation of* $\Delta\langle\rho^2\rangle$

Corresponding to the different criteria applied for the definition of the pseudocritical $\beta_{Hc}(L)$ we obtain histograms of the various operators just at the respective pseudo–criticality. From the jump of the operator expectation values between the phases (read off from the maxima of the corresponding histogram) an infinite volume extrapolation is performed. A collection of discontinuities of $\langle\rho^2\rangle$ and $\langle\rho^4\rangle$ for various finite lattices is shown in Figs. 7 and 8. As in the analysis of Ref. [7] we found that the size dependence of the jumps for all available lattice sizes is best described by a $1/L^2$ fit. The extrapolations to infinite volume (for the two criteria $B_{\rho^2}$ and $C_{\rho^2}$) and the averages (of the results obtained with different methods to extrapolate) of the jumps of the scalar Higgs operators are given in table 4 in lattice units.

The corresponding condensate discontinuities in continuum units are collected in table 5. The quadratic Higgs condensate is already independent of finite $a$ effects. On the contrary, the quartic condensate shows a severe $a$ dependence. So we conclude, it is more subtle to extract an appropriate continuum value for this higher condensate.
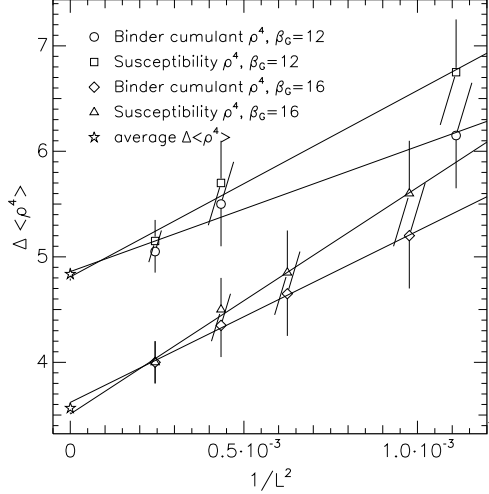
16

Figure 8: *Infinite volume extrapolation of* $\Delta\langle\rho^4\rangle$

| | $B_{\rho^2}$ | $C_{\rho^2}$ | average |
|---|---|---|---|
| $\Delta\langle\rho^2\rangle$ | | | |
| $\beta_G = 12$ | 0.490(9) | 0.479(8) | 0.485(6) |
| $\beta_G = 16$ | 0.372(8) | 0.362(7) | 0.367(5) |
| $\Delta\langle\rho^4\rangle$ | | | |
| $\beta_G = 12$ | 4.86(9) | 4.81(8) | 4.84(6) |
| $\beta_G = 16$ | 3.62(8) | 3.51(7) | 3.56(5) |

Table 4: Infinite volume limit for $\Delta\langle\rho^2\rangle$ and $\Delta\langle\rho^4\rangle$ at $M_H^* = 70$ GeV

| | $\Delta\langle\phi^+\phi\rangle/g_3^2$ | $\Delta\langle(\phi^+\phi)^2\rangle/g_3^4$ |
|---|---|---|
| $\beta_G = 12$ | 0.250(3) | 1.28(2) |
| $\beta_G = 16$ | 0.250(4) | 1.65(3) |

Table 5: The continuum Higgs condensate discontinuities at $M_H^* = 70$ GeV

For the case of the lighter Higgs mass $M_H^* = 35$ GeV we present the corresponding quantities in table 6. These data were obtained from two separate, completely metastable runs on a $40^3$ lattice at $\beta_G = 12$ and $\beta_H = 0.34140$. They failed to tunnel to the other phase. The actual $\beta_H$ value of these two runs had been found as pseudocritical one on a smaller lattice.

Besides of jumps in the quadratic and quartic Higgs condensates also a discontinuity in the expectation values of $E_{link}$ appears being a good indicator

17

| | |
|---|---|
| $\Delta\langle\rho^2\rangle$ | 6.24(1) |
| $\Delta\langle\rho^4\rangle$ | 96.1(2) |
| $\Delta\langle\phi^+\phi\rangle/g_3^2$ | 3.20(1) |
| $\Delta\langle(\phi^+\phi)^2\rangle/g_3^4$ | 25.2 (1) |

Table 6: $\Delta\langle\rho^2\rangle$ and $\Delta\langle\rho^4\rangle$ and condensates at $M_H^* = 35$ GeV and $\beta_G = 12$

for the phase transition as well.

It is known (see [17]), that the sum of expectation values of the various Higgs operators is constant according to a sort of Schwinger–Dyson equation

$$-3\beta_H \langle E_{link}\rangle + (1 - 2\beta_R)\langle\rho^2\rangle + 2\beta_R \langle\rho^4\rangle = C \tag{21}$$

independent of the couplings $\beta_H$, $\beta_G$ and $\lambda_3/g_3^2$. We have checked this sum rule for all used coupling values and found $C = 2$ exactly within very good numerical accuracy.

From eq. (21) one sees that the Higgs condensate discontinuities are related to each other by the following sum rule

$$-3\beta_H \Delta\langle E_{link}\rangle + (1 - 2\beta_R)\Delta\langle\rho^2\rangle + 2\beta_R \Delta\langle\rho^4\rangle = 0. \tag{22}$$

Additionally, the expectation value of the average plaquette $\langle P\rangle$ shows a discontinuity as well at the phase transition. The jump in this observable is numerically a tiny effect at the larger Higgs mass (mostly superimposed by the fluctuations, see the discussion and Fig. 10 below). Nevertheless, we are able to estimate this jump using the phase separation technique discussed earlier.

In table 7 the jump $\Delta\langle P\rangle$ is reported for $\beta_H$ values nearest to the critical ones at $M_H^* = 70$ and 35 GeV at lattice sizes $64^3$ and $40^3$, respectively. At the

| | | $\Delta\langle P\rangle$ |
|---|---|---|
| $M_H^* = 70$ GeV | $\beta_G = 12$ | 0.00037 |
| | $\beta_G = 16$ | 0.00015 |
| $M_H^* = 35$ GeV | $\beta_G = 12$ | 0.00370 |

Table 7: Estimated plaquette jump $\Delta\langle P\rangle$

larger $M_H^*$ the phase separation technique is used. We do not set these jumps in correspondence to a continuum gauge condensate discontinuity

$$\Delta\langle\frac{1}{4}F_{\alpha\beta}^a F_{\alpha\beta}^a\rangle/g_3^6 = -3\frac{\beta_G^4}{64}\Delta\langle P\rangle \tag{23}$$

18

since severe $a$ effects and perturbative contributions are expected.

## 5.2   Latent heat

The latent heat $L_{heat} = \Delta\epsilon$ ($\epsilon$ is the density of thermal energy) of the transition is calculated according to [17]

$$\frac{L_{heat}}{T_c^4} \quad = \quad \frac{M_H^2}{T_c^3}\,\Delta\langle\phi^+\phi\rangle \qquad\qquad (24)$$

With the reported jumps and the values for $M_H$ and $T_c$ ($g^2(\mu_{T_c}) \approx 0.38$) we find the latent heats at the higher and smaller Higgs masses as given in table 8.

| | $L_{heat}/T_c^4$ |
|---|---|
| $M_H^* = 70$ GeV | 0.0176(3) |
| $M_H^* = 35$ GeV | 0.180(1) |

Table 8:   Latent heat

The equal weight method makes it possible to reconstruct directly the free energy densities of the pure phases in the vicinity of the phase equilibrium. The corresponding numbers are obtained in the iterative search of the pseudocritical $\beta_{Hc}$ using the reweighting technique at fixed $\beta_G$. The latent heat can then be expressed alternatively as the jump $\Delta\epsilon$ of the energy density by

$$\frac{L_{heat}}{T_c^4} = \frac{1}{T_c^2 a^3 L^3}\frac{d}{dT}\Big(\log w_s - \log w_b\Big)\Big|_{T=T_c}. \qquad\qquad (25)$$

Using at fixed $\beta_G$

$$\frac{d}{dT}\Big|_{T=T_c} \approx -\beta_{Hc}^2\frac{a^2 M_H^2}{2T_c}\frac{\partial}{\partial\beta_H}\Big|_{\beta_H=\beta_{Hc}} \qquad\qquad (26)$$

one finds

$$\frac{L_{heat}}{T_c^4} = -\frac{g_3^2}{T_c^3}\frac{1}{8}M_H^2\beta_{Hc}^2\beta_G\;\frac{1}{L^3}\frac{\partial}{\partial\beta_H}\Big(\log w_s - \log w_b\Big)\Big|_{\beta_H=\beta_{Hc}}. \qquad\qquad (27)$$

The change of the weights very close to the critical $\beta_H$ is shown in Fig. 9. Taking the corresponding slopes needed in (27) we obtain at $M_H^* = 70$ GeV

for the largest lattices (where the equal weight method can be applied without ambiguity) $L_{heat}/T_c^4 = 0.0180(9)$ which is in good agreement with the other method.
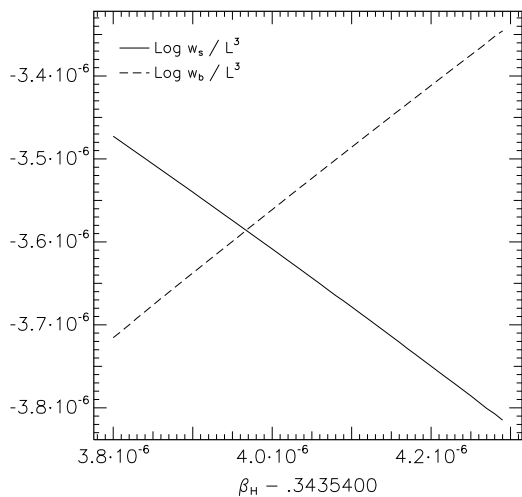


Figure 9: *Weights for the pure phases around the equal weight pseudocritical* $\beta_H$ *for* $\beta_G = 12$ *on a* $64^3$ *lattice*

## 5.3  Wilson loops at the phase transition

If the lattice is large enough, a two–state signal becomes visible also in the average plaquette $P$. This can be seen in Fig. 10 for $\beta_G = 12$, $\beta_H = 0.343548$ at $64^3$. 120.000 measurements are collected in this histogram.

For medium size rectangular Wilson loops a two–state signal is even better visible than for the plaquette. This is due to the fact that the configuration averages follow an area and perimeter law in the symmetric and broken phase, respectively. If these loops are not too large (*i.e.* not too small numerically), this can be well separated in the histograms of Wilson loops as demonstrated in Fig. 11. In that figure a histogram of 2.000 measurements of a space–averaged Wilson loop of size $12 \times 12$ is shown obtained during 20.000 MC iterations in the metastability region at lattice size $48^3$. The corresponding average plaquette for this size does not show a two–state signal.

In Fig. 12 we plot the logarithm of expectation values of symmetric $L \times L$ Wilson loops versus area $A = L^2$, separated into symmetric and broken phase contributions at the critical $\beta_H$, for both Higgs masses $M_H^* = 70$ GeV and 35
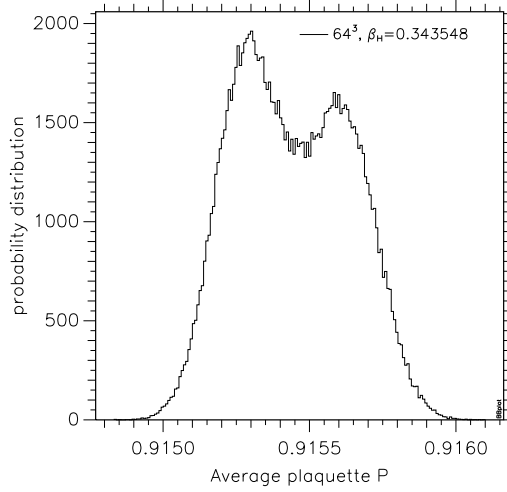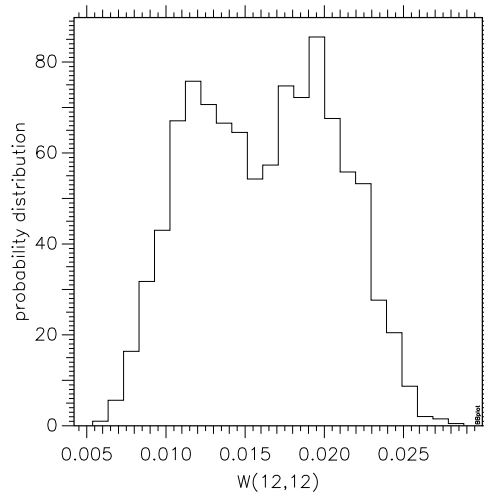
20

Figure 10: *Measured histograms of P for* $\beta_G = 12$



Figure 11: *Measured histogram of the* $12 \times 12$ *Wilson loop*

GeV (in both cases for $\beta_G = 12$). The numbers of measurements are 2.000 in both cases. This figure shows clearly the area law in the symmetric phase and practically no (or only weak) dependence of the string tension (in lattice units) on the Higgs self–coupling $\lambda_3$.
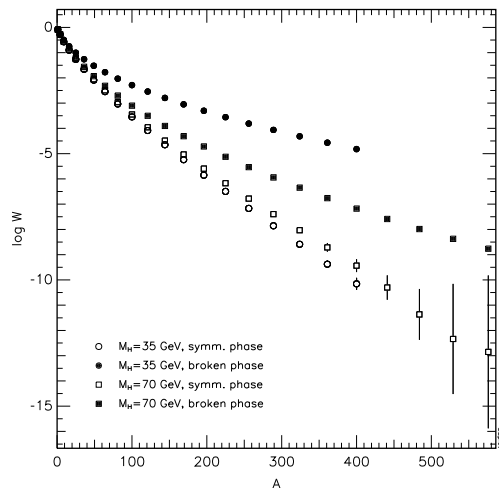
Figure 12: *Wilson loops for* $\beta_G = 12$

## 5.4    Estimate of the surface tension

The coexistence of both phases in lattice configurations opens the possibility to determine the surface tension $\alpha$. The use of the equal weight method as described above allows to estimate the contribution of the mixed phase state at the pseudocritical coupling for which $w_b = w_s$ (for large enough lattices). The mixed phase state weight $w_{mix}$ is directly related to $\alpha$. Using these weights to estimate $\alpha$ seems to be more natural than to obtain the surface tension from the ratio of the maximum to the minimum of the $\rho^2$ distribution at equilibrium defined by equal weight. For asymmetric transitions the choice of the maximum is even somewhat arbitrary (unless *equal height* is the criterium of choice).

To get an idea about the shape of the interfaces (bubbles, walls) we show a snapshot of a particular configuration on a $32^2 \times 128$ ($M_H^* = 70$ GeV, $\beta_G = 12$) in the pseudocritical $\beta_H$ region. This configuration has a $\rho^2 = 3.67$ where mixed states can be expected. To suppress the large fluctuations in the local $\rho_x^2$ values we have averaged them iteratively over the next neighbours. The configuration obtained in this way is shown in Fig. 13 where we have plotted all lattice points with $\rho_x^2 > 3.67$. The filled (empty) region can be interpreted as the broken (symmetric) phase contribution. Besides of a few bubbles we see two large interfaces separating the pure phases. Although the configuration has been smoothed the interfaces are rather structured which makes it difficult to assign them a definite area $A$. For simplicity we use in the fit below $A = L_x^2 a^2$, which tends to overestimate $\alpha$.

22

Figure 13: *Smoothed mixed state configuration, plotted are the points to be assigned to the broken phase*

We parametrize the relation between the weights at pseudocriticality and $\alpha$ for lattices of the form $L_x^2 \times L_z$ as follows

$$\frac{w_{mix}}{w_s} = \frac{w_{mix}}{w_b} = b \; L_z^2 \; \log L_x \exp\left(-2\alpha a^2 L_x^2/T_c\right). \tag{28}$$

With that ansatz we try to describe data obtained either from cubic and from cylindrical lattice geometries.

The factor $L_z^2$ is an entropy factor which accounts for the positions of the two surfaces, $\log L_x$ is the result (for $d = 3$) of the capillary wave approximation for the (internal) fluctuations of the surfaces. The degeneracy factor $b$ is introduced to count different possible orientations of the surfaces dominant for cubic ($b = 3$) and for prolongated lattices ($b = 1$).

In Fig. 14 we present the data for $\alpha/T_c^3$ as function of $(\beta_G/L_x^2)$ for various lattice sizes and geometries and different $\beta_G$ values at $M_H^* = 70$ GeV. From a linear fit to the infinite volume limit we find the upper bound

$$\frac{\alpha}{T_c^3} \approx 0.00022. \tag{29}$$

These lattice results are smaller by one order of magnitude than the one–loop estimates for the surface tension [23]. A trend of finding smaller surface tensions at larger Higgs masses was already observed in [7]. Whereas the latent heat is determined by the position of the broken minimum alone, the surface tension is sensitive to the shape of the effective potential in the whole $\varphi$ range between the symmetric and the broken phase. The disagreement between the measured surface tension and the one–loop estimate at intermediate Higgs mass appears to indicate that the loop expansion to the effective potential gets out
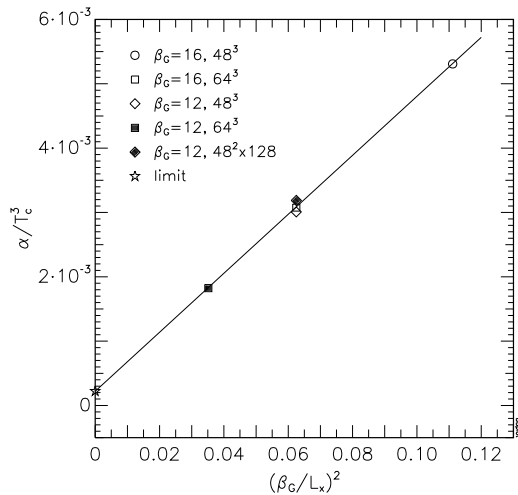
Figure 14: *Surface tension vs. $(\beta_G/L_x)^2$*

of control at intermediate $\varphi$ values already, reflecting the infrared problems of the symmetric phase.

The surface tension is the only quantity indicating a substantial deviation from perturbative predictions at $M_H^* = 70$ GeV, *i.e.* additional weakening of the phase transition with increasing Higgs mass. At still larger Higgs masses ($M_H \geq M_W = 80$ GeV) the phase transition has been suggested recently to be of second order [15] or to be a smooth crossover [16] in accordance with predictions from the study of gap equations [14]. The first case would be difficult to discriminate from a phase transition being very weakly first order. In any case, however, one will observe the turn–over to a very weak or continuous transition at higher Higgs mass.

# 6   Broken phase and perturbation theory

Analysing the lattice data one should answer the question whether the broken phase can be understood perturbatively. There are no infrared problems in this phase because the elementary excitations are massive. Nevertheless, a perturbative treatment is expected to break down at larger Higgs masses, close to the phase transition.

It is known [24] that for calculating the temperature dependent effective

potential the appropriate effective expansion parameter for the broken phase is

$$g_{3\,eff}^2 = \frac{g_3^2}{2m_W(T)} \tag{30}$$

with the 3–dimensional gauge boson mass $m_W(T)$. This coupling can be determined from the two–loop effective potential [25]. Its value depends on the gauge fixing as well as on the choice of the renormalization point $\mu_3$. Using Feynman gauge and $\mu_3 = g_3^2$ for $M_H^* = 70$ GeV this effective coupling is found to be 1.10 at the critical temperature.

In Figs. 15 and 16 we present a comparison of our lattice data with two–loop continuum predictions for the renormalized Higgs condensate $\phi^2(T)$ and the vector boson ($m_W(T)$) and Higgs boson ($m_H(T)$) masses at the corresponding temperature, respectively, using the effective potential [25]. The temperature $T$ is implicitly given via $m_3^2(g_3^2)$ (see eqs. (3, 4, 5). The $\langle\phi^2\rangle$ data are obtained from the measured $\langle\rho^2\rangle$ by subtracting the one–loop and two–loop counterterms [17]
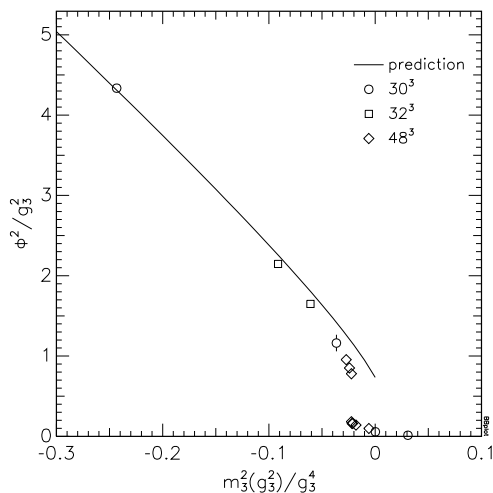


Figure 15: *Comparison of perturbative and lattice $\phi^2$*

$$\phi^2 = 2\langle\phi^+\phi\rangle(g_3^2),$$
$$\langle\phi^+\phi\rangle(g_3^2)/g_3^2 = \frac{1}{8}\beta_G\,\beta_H\,\langle\rho^2\rangle - \frac{\beta_G}{8\pi}\Sigma - \frac{3}{16\pi^2}\Big(\log\frac{3}{2}\beta_G + 0.67\Big). \tag{31}$$

We differ from [7] by a factor of 2 in the convention of defining $\phi^2$. The two–
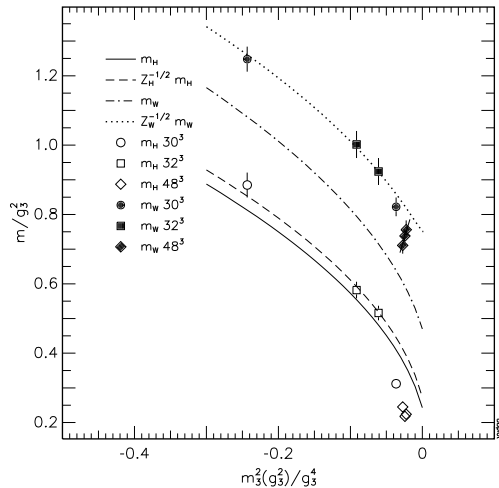
Figure 16: *Measured masses at* $M_H^* = 70$ *GeV and* $\beta_G = 12$ *compared to continuum perturbation theory*

loop predictions are calculated in Feynman gauge. In the case of $m_W$ and $m_H$ predictions are shown with and without the one–loop wave function renormalization constants for the Higgs and vector boson masses $Z_H$ and $Z_W$ [24] $(m = Z^{-1/2} m_0)$. The prediction for $m_H$ is derived from the curvature of the effective two–loop potential at the broken minimum, which is not identical to the pole mass. However, the difference is expected to be small.

Comparing perturbation theory predictions with the data we observe very good agreement deeper in the broken phase, as should be expected. Wave function renormalization is obviously required. Otherwise the agreement is poor. Close to the phase transition we observe a systematic difference between lattice data and the continuum calculation as function of $m_3^2$. Nevertheless, the predicted mass and $\langle \phi^2 \rangle$ values at the corresponding continuum critical point agree well with the measured ones at $T_c$ ($m_3^2 < 0$). The mapping of the two–loop results from the parameter $v_0/v$ used in [25] to $m_3^2(g_3^2)$ fails close to the phase transition. This may be an indication that higher loop terms start to play a significant role in this regime.

# 7   Some properties of the symmetric phase

3–dimensional $SU(2)$ pure gauge theory is known to possess confinement, *i.e.* the spectrum is formed by massive $W$–balls instead of the elementary massless

26

$W$'s. Adding a Higgs doublet has similar consequences as adding fermions: new massive ($\phi^+\phi$) bound states occur, and the static confining potential should be screened. The Lagrangian mass of the scalar bosons increases with temperature, i.e. sufficiently away from the phase transition the Higgs bound states become heavy. As a consequence, the symmetric phase should more and more resemble pure $SU(2)$ gauge theory at higher and higher temperature. In the $\beta_H$ range (resp. $m_3$ range) that we have explored this could not yet be confirmed, however. The lowest Higgs bound state is still significantly lighter than the lightest $0^+ W-$ ball.

## 7.1 Higgs and vector boson bound states

Results for the lowest Higgs bound state ($0^+$) and the vector boson bound state ($1^-$) are shown in Fig. 17 as function of $m_3(g_3^2)/g_3^4$. Data from different $\beta_G$
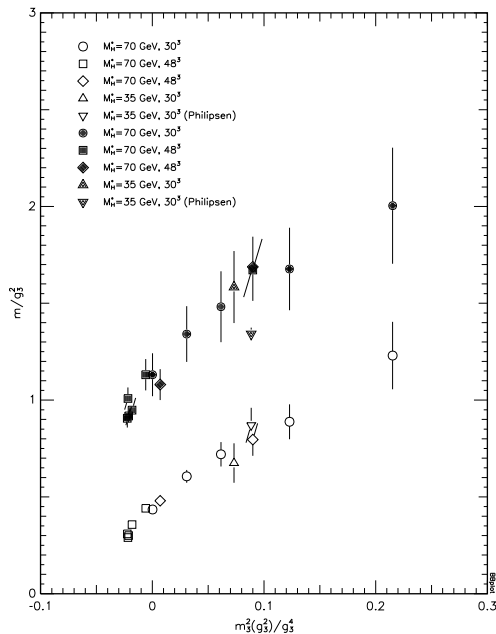


Figure 17: *Masses in the symmetric phase for $\beta_G = 12$, diamonds correspond to $\beta_G = 16$*

values nicely coincide. Our results for the vector boson mass $m_W$ should be considered as upper bounds, because of a possible admixture of states with a somewhat higher mass. For the Higgs mass $m_H$ this problem is not severe because the mass gap to higher mass states is significantly larger. This problem

has been carefully studied recently by Philipsen et al. [26]. Note that our gauge boson masses are calculated from correlators of gauge invariant operators in contrast to Ref. [15] where gauge variant correlators have been analysed, obtained in conjunction with gauge fixing (Landau gauge).

One important conclusion from Fig. 17 is the scaling behaviour of masses when plotted versus $m_3^2$. Outside the immediate vicinity of the phase transition no $\lambda_3$ dependence is seen within errors. Our data point at the lighter Higgs mass has been reanalysed as compared to our Ref. [6].

An attempt has been made to reproduce these bound state masses by approximate analytical methods [27] based on the Feynman–Schwinger representation of correlators. The measured static potential (see below) is used as input. The level spacings ($2s$–$1s$, $1p$–$1s$) are very well reproduced by this approach for the data point of Ref. [26]. The other interesting phenomenon is the $m_3^2$ dependence of the bound state masses, also being reproduced well.

## 7.2   The static potential

In four dimensions one usually considers Creutz ratios of Wilson loop expectation values instead of the loops directly in order to avoid explicit renormalization. This is not necessary in three dimensions because renormalization becomes very simple. All ultraviolet divergent contributions are covered by the exponentiated (Abelian) one–loop term, having a logarithmic divergence. For the potential, the one–loop massless $W$–exchange contribution is $g_3^2\, 3/(8\pi)\log(R/(2a))$. This is the result of a continuum calculation with $a$ introduced as ultraviolet cut–off. Interesting enough, the behaviour of the two–loop contribution can simply be predicted on dimensional grounds to be $c_{2l}g_3^4 R$, with some constant $c_{2l}$ not yet evaluated. Correspondingly, higher loop orders generate higher powers of $R$. Perturbation theory will therefore be appropriate to describe small Wilson loops, *i.e.* the potential at small $R$, whereas it breaks down in a power–like manner at large distances (infrared regime). This is different from the $4d$ case where corresponding effects are logarithmic.

At small $R$, an appropriate fit to the potential (in units of $g_3^2$) should be provided by

$$V(R) = V_1 + \frac{3}{8\pi} \log(\frac{R}{2a}) + c_1 R, \tag{32}$$

where $a$ is identified as the lattice constant, and $V_1$ has been introduced as additional fit parameter. It could be fixed, however, by a one–loop lattice calculation (not yet done). The renormalized potential will anyway contain some

arbitrariness in the overall normalization, due to the choice of the renormalization point.

A priori, it is not clear up to which distance this ansatz may be appropriate. Interesting enough we shall find (see below) that it describes our data reasonably well in the whole range, up to about $R = 6/g_3^2$. Two–loop perturbation theory generates a term looking like a string tension. The value of $c_1$ fitted at intermediate $R$ may therefore have perturbative as well as non–perturbative contributions. Because of the gauge coupling being dimensionful it will be difficult not only in practice but also conceptually to separate perturbative from non–perturbative effects. This in particular concerns the definition of a possible $W$ condensate.

Equation (32) is based on massless perturbation theory. We know, however, that the symmetric phase is formed by massive bound states instead. This information may be taken into account in fitting our potential data. We shall also consider the ansatz ($K_0$ is a modified Bessel function)

$$V(m, R) = V_2 - \frac{3}{8\pi} K_0(mR) + c_2 R \qquad (33)$$

with some additional fit parameter $m$ representing the mass of the exchanged particle. It should come out close to the measured $W$ mass.
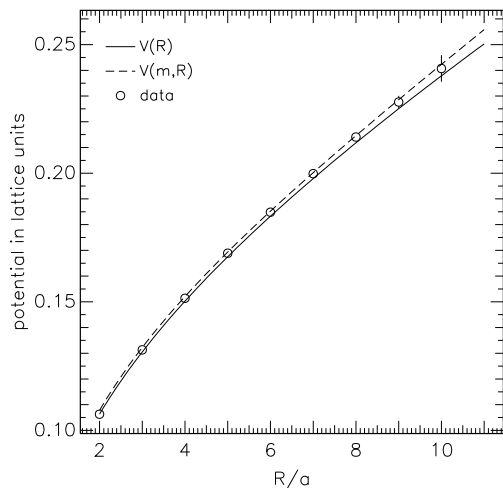


Figure 18: *Example for static potential in comparison to perturbation theory*

As an example we present in Fig.18 the potential for $\beta_H = 0.3434$, $\beta_G = 12$ and $M_H^* = 70$ GeV from a run on a $30^3$ lattice. The data for $V(R)$ are obtained

29

from exponential fits to the Wilson loops

$$W(R/a, T/a) = C(R)\exp(-V(R)T) \ , \quad 2a \leq R \leq T - 3a. \qquad (34)$$

This potential is compared to the above described ansätze using massless ($m = 0$) and massive ($m > 0$) perturbation theory. For the second case the mass parameter is chosen to minimize the $\chi^2$ value of the least square fit. For this particular example we obtain the parameter values $V_1 = 0.267$, $c_1 = \sigma/g_3^2 = 0.0791g_3^2$ for the massless and $V_2 = 0.339$, $c_2 = \sigma/g_3^2 = 0.118g_3^2$, $m = 0.93g_3^2$ for the massive case ($m_3^2(g_3^2)/g_3^4 = 0.00022$). In general, the fits using massive perturbation theory ansatz seem to describe the data somewhat better at the larger distances studied.

## 7.3 Temperature and Higgs mass dependence of the "string tension"

In Fig. 19 we present the string tension obtained from the ansätze for the potential in (32) and (33), respectively, at different $m_3^2$ values. In this analysis
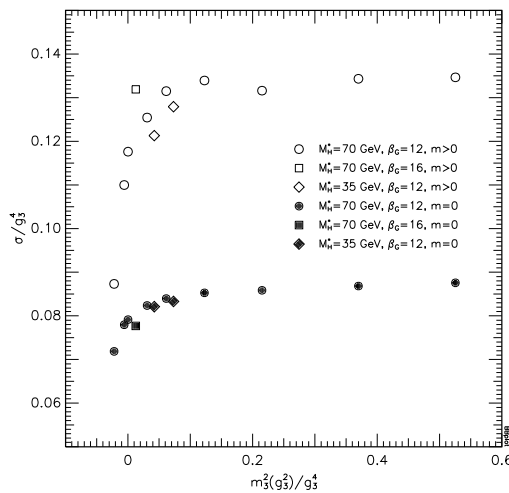


Figure 19: *String tension* $\sigma/g_3^4$ *from (32) and (33) vs.* $m_3^2(g_3^2)/g_3^4$

data from the higher and smaller Higgs mass $M_H^*$ cases as well as for different $\beta_G$ are used. Most of the data are from $30^3$ lattices. The closest to $T_c$ and the $\beta_G = 16$ string tensions are obtained from fits to Wilson loops on $48^3$ lattices (compare Fig. 12) up to distances $R = 18a$. The scattering of the data points

is an estimate for the error of the string tension. The errors obtained from the least square fit are obviously too small to be reliable.

We observe that there is no significant dependence of $\sigma/g_3^4$ on $\lambda_3$ ($M_H^*$) in both fits. At larger $m_3^2$ (temperatures), *i.e.* deeper in the symmetric phase, the result of the string tension based on the fit to massive perturbation theory (33) is (not unexpectedly) close to the value reported by Teper [28] for pure $3d$ $SU(2)$ gauge theory. This lends additional support to this parametrization of the potential.

For the lattice distances we could explore the expected screening behaviour of the static potential has not yet been observed. Still larger distances are difficult to study due to the numerical smallness of the Wilson loops that are needed.

# 8 Summary

The numerical results of this study provide evidence for the first order nature of the thermal phase transition in the $SU(2)$–Higgs system with Higgs masses up to 70 GeV. The answers will soon converge concerning the upper critical Higgs mass above which the thermal transition is no longer first order.

One of the motivations for the interest in non–perturbative investigations of the thermal electroweak phase transition in general, was to be able to check the reliability of perturbative calculations of the effective potential. The corresponding results of two–loop perturbation theory are confirmed for the masses and the renormalized Higgs condensate in the broken phase. It turns out, that the effect of wave function renormalization cannot be ignored. Physics that depends only on the potential in the vicinity of the broken minimum, can be systematically improved by higher order perturbation theory.

The surface tension which is sensitive to the barrier shape of the effective potential for Higgs field below the order parameter at $T_c$ is systematically overestimated in the perturbative calculation available so far. But this is not exclusively a problem for perturbation theory. The surface tension is notoriously hard to measure for weak transitions as at $M_H \simeq 70$ GeV. The equilibrium configurations can be inspected and show rather structured interphase surfaces. In view of this, estimators of the surface tension like ours seem to be not extremely justified either.

To check the viability of the dimensional reduction program in the vicinity of the electroweak phase transition has been another motivation for $3d$ lattice studies. The reduced model does not only make very precise predictions, but

seems to be reliable in the range of Higgs masses which was of particular interest in this investigation. In order to learn about the necessity to include higher dimensional operators into the effective lattice action one should explore the case of smaller or very much heavier Higgs masses, but this is much less interesting, phenomenologically. In any case, $4d$ anisotropic lattices will be important for obtaining results (and to study masses) near to the continuum limit in physically large 3–volumes.

Phenomenologically, the Standard Model is ruled out as an arena for baryon asymmetry generation at the electroweak transition. The $3d$ lattice approach promises to be applicable as an effective formulation of nonstandard extensions as well. The phase structure of the model, once fully reveiled by $3d$ lattice simulations, as well as the quantitative characterization of the strength of the phase transition, will be useful to inquire a multitude of $4d$ extended theories by Monte Carlo parameter exploration. For this purpose, it is now possible to go beyond the easiest perturbative formulae.

We have turned the equal weight criterion in conjunction with the multihistogram Ferrenberg–Swendsen interpolation technique into a valuable iterative procedure. In our variant to apply this criterion, we do not need to choose any *a priori* known cut between the phases nor to associate individual configurations uniquely to one of the pure phases or to the two–phase mixed configurations. Finally, the method yields the thermodynamical weight of the latter ones. For any lattice size where the pure phase histograms do not overlap, the critical hopping parameter is obtained within the cone of infinite volume extrapolations of all other, more standard criteria to find $\beta_{Hc}$. Moreover, the iterative search for $\beta_{Hc}$ provides the thermal energy of both pure phases in the vicinity of the transition, allowing to obtain an independent estimator for the latent heat.

We have put much more emphasis than before to the properties of the symmetric phase. Within the $3d$ approach, information on the spectrum of particle like states can only be accessed through the $3d$ correlation lengths. The pattern obtained lacks deeper understanding. Despite some technical progress in resolution of the spectrum of the $3d$ transfer matrix, the interplay between the confining properties of the $3d$ effective theory at high physical temperature and the space–time structure of physical excitations needs further investigations, as well as the nature of this confinement itself for the $3d$ pure gauge theory and in the presence of scalar matter fields.

# Acknowledgements

# References

[1] B. Bunk, E.-M. Ilgenfritz, J. Kripfganz and A. Schiller, Phys. Lett. **B284** (1992) 371; Nucl. Phys. **B403** (1993) 453

[2] Z. Fodor, J. Hein, K. Jansen, A. Jaster, I. Montvay, Nucl. Phys. **B439** (1995) 147

[3] E.-M. Ilgenfritz and A. Schiller, Nucl. Phys. **B** (Proc. Suppl.) **42** (1995) 578

[4] K. Farakos, K. Kajantie, K. Rummukainen and M. Shaposhnikov, Nucl. Phys. **B407** (1993) 356

[5] K. Farakos, K. Kajantie, K. Rummukainen, M. Shaposhnikov, Phys. Lett. **B336** (1994) 494

[6] E.-M. Ilgenfritz, J. Kripfganz, H. Perlt and A. Schiller, Phys. Lett. **B356** (1995) 561

[7] K. Kajantie, M. Laine, K. Rummukainen and M. Shaposhnikov, CERN-TH/95-263 (1995)

[8] M. Gürtler, E.-M. Ilgenfritz, J. Kripfganz, H. Perlt and A. Schiller, hep-lat/9512022

[9] D.A. Kirzhnits and A.D. Linde, Phys. Lett. **72B**, 471

[10] W. Buchmüller, Z. Fodor, T. Helbig and D. Walliser, Ann. Phys. **234** (1994) 260

[11] J.M. Cline, K. Kainulainen, CERN-TH/96/20 (1996)

[12] M. Losada, RU-96-25 (1996)

[13] M. Laine, Heidelberg preprint HD-THEP-96-13

[14] W. Buchmüller and O. Philipsen, Nucl. Phys. **B443** (1995) 47

[15] F. Karsch, T. Neuhaus, A. Patkós and J. Rank, Bielefeld preprint BI-TP 96/10

[16] K. Kajantie, M. Laine, K. Rummukainen and M. Shaposhnikov, CERN-TH/96-126 (1996)

[17] K. Farakos, K. Kajantie, K. Rummukainen and M. Shaposhnikov, Nucl. Phys. **B425** (1994) 67; **B442** (1994) 317

[18] K. Kajantie, M. Laine, K. Rummukainen and M. Shaposhnikov, Nucl. Phys. **B458** (1996) 90

[19] M. Laine, Nucl. Phys. **B451** (1995) 484

[20] G. Parisi, R. Petronzio and F. Rapuano, Phys. Lett. **128B** (1983) 418

[21] A.M. Ferrenberg and R.H. Swendsen, Phys. Rev. Lett. **61** (1988) 2635; **63** (1989) 1195

[22] S. Kappler and C. Borgs, Int. J. Mod. Phys. **C3** (1992) 1099

[23] J. Kripfganz, A. Laser and M.G. Schmidt, Heidelberg preprint HD-THEP-95-53, Z. Phys. to appear

[24] J. Kripfganz, A. Laser and M.G. Schmidt, Nucl. Phys. **B433** (1995) 467

[25] J. Kripfganz, A. Laser and M.G. Schmidt, Phys. Lett. **B 351** (1995) 266

[26] O. Philipsen, M. Teper and H. Wittig, DESY preprint DESY-96-017

[27] H.G. Dosch, J. Kripfganz, A. Laser, M.G. Schmidt, Phys.Lett. **B365** (1996) 213; and paper in preparation

[28] M. Teper, Phys. Lett. **B289** (1992) 115; **B311** (1993) 223